AIChE WILEY InterScience DISCOVER SOMETHING GREAT

Multiobjective Optimization of Semibatch Reactive Crystallization Processes

Debasis Sarkar, Sohrab Rohani, and Arthur Jutan
Dept. of Chemical & Biochemical Engineering, University of Western Ontario, London, Ontario, Canada N6A 5B9

DOI 10.1002/aic.11142
Published online March 27, 2007 in Wiley InterScience (www.interscience.wiley.com).

The determination of the optimal feed profiles for a reactive crystallizer is an important dynamic optimization problem, as the feed profiles offer a significant control over the quality of the product crystals. Crystallization processes typically have multiple performance objectives and optimization using different objective functions leads to significantly different optimal operating conditions. Therefore, a multiobjective approach is more appropriate for optimization of these processes. The potential for multiobjective optimization approach is demonstrated for semibatch reactive crystallization processes. The multiobjective approach usually gives rise to a set of optimal solutions, largely known as Pareto-optimal *solutions. The Pareto-optimal solutions can help the designer visualize the trade-offs between different objectives, and select an appropriate operating condition for the process. A well known multiobjective evolutionary algorithm, the elitist nondominated sorting genetic algorithm, has been adapted to illustrate the potential for the multiobjective optimization approach.* © 2007 American Institute of Chemical Engineers *AIChE J,* 53: 1164–1177, 2007
Keywords: semibatch, reactive crystallization, precipitation, dynamic simulation, multiobjective optimization, genetic algorithm

Introduction

Reactive crystallization or precipitation is a key production step for a wide range of chemical and pharmaceutical industries to produce solid particles with desirable characteristics, such as large crystal size, narrow crystal-size distribution (CSD), high-yield, and so on. During a semibatch reactive crystallization, two liquid reactants are brought into close contact in a single jet or double jet operation, and the crystalline product or precipitate is formed by a chemical reaction in concentrations exceeding the solubility of the solute (supersaturation). If the chemical reaction is fast, and the solubility of the product crystal is low compared to the reactant concentrations, the supersaturation at the feed point becomes high, which results in rapid nucleation and fast crystal growth. Thus, the mixing mechanism and the feed flow rates of the reactants exert significant influence on the characteristics of the product crystals, and an optimized crystallization process is required to produce a desired CSD.

There has been extensive research on the experimental, as well as theoretical aspects of reactive crystallization processes.[1–10] However, most studies on reactive crystallization processes have concentrated on reaction kinetics and influence of mixing on mean-particle size, size distribution and morphology. Results published on the influence of the stirring rate and the feed rate on the mean-crystal size in semibatch reaction crystallization processes are reviewed by Torbacke and Rasmuson.[11] Not very much research has been directed toward mathematical optimization of reaction crystallization processes. Semibatch operation for a reactive crystallization process offers the advantages of easily controllable feed rates, which can lead to significant improvement in product quality than traditional batch operation. Tavare and Garside[12] simulated a general reactive process in a semibatch crystallizer and concluded that variations in the reactant addition profiles can be used to exercise significant control over the product-size distribution. Mukhopadhyay and Epstein[13] also reported in their simulation study that the feed flow rate

Correspondence concerning this article should be addressed to S. Rohani at rohani@eng.uwo.ca.

is an important control variable to improve the product characteristics for a semibatch evaporative crystallization process. Experimental studies by Philips et al.[14] on barium sulfate precipitation, and by Torbacke and Rasmuson[10] on benzoic acid crystallization, show that the feed rates do affect the final product CSD in semibatch reaction crystallization processes. Recently, Choong and Smith[15] presented a stochastic optimization framework, based on Simulated Annealing for optimizing semibatch reactive crystallization processes. The optimization is sought with respect to the reactants feed profiles that maximize the crystal size subject to a specified maximum coefficient of variation (CV), or minimize CV subject to a specified minimum crystal size.

Crystallization processes typically have multiple performance objectives (large crystal size, narrow CSD, high-yield, and so on), which are often conflicting in nature. It is desirable to have a product CSD that simultaneously satisfies several such objectives, if possible. For example, it would be desirable to have a product CSD with a large weight mean size (WMS), and a small CV in a minimum time of operation. Choong and Smith[15] reported that optimization with different objective functions leads to different optimal feed profiles and initial amounts of reactants. The control strategies that produce the largest average crystal size usually lead to high CV, and there is a trade-off between the performance objectives. Such optimization problems, thus, require simultaneous consideration of multiple objectives in order to thoroughly explore the potential of various operating policies. Recently, Sarkar et al.[16] presented a comprehensive study on multiobjective optimization of seeded batch-crystallization processes. It has been shown that a wide range of alternative solutions that trade different objectives against each other is identified when a multiobjective methodology is employed for the optimization of such processes, and the knowledge of such multiple optimal solutions helps a decision maker to make a better choice of the desired design and operating conditions. In this contribution, we extend this methodology of multiobjective optimization to semibatch reactive crystallization processes, and the efficiency of the methodology is illustrated by solving two multiobjective optimal control problems that are related to such processes.

It may be pointed out here that the case studies considered here treat the crystallizers as well-mixed systems. In a large scale precipitation or reactive crystallization process, the assumption of a homogeneous solution at the molecular and even at the macroscale is far from the truth. Depending on the mode of operation and operating conditions, mixing may become the rate-controlling step for fast precipitation systems. The intent of this communication, however, is to study the multiobjective optimization of a reactive crystallization process, which has never been reported in the literature. Adding an extra dimension of complexity by incorporating the micromixing and macromixing models would certainly distract the main focus of the paper. Many studies have been conducted to investigate the effect of feed position, the diameter of the feed-pipe, the feeding rate and profile, the hydrodynamic within the vessel, and the time of feeding on the CSD in reactive crystallization processes. Experimental studies show that feed rates do have an effect on the final product CSD in such process.[10,14,17] In addition, under certain conditions the importance of mixing, and in particular, the effects of micromixing can be neglected. Therefore, in the present study, we will assume a well-mixed system, in order to focus on the multiobjective optimization problem.

Multiobjective Optimal Control Problems

Let us consider a reactive crystallization process described by the following state equations

$$\frac{d\mathbf{x}}{dt} = \mathbf{f}(\mathbf{x}, \mathbf{u}) \tag{1}$$

with the initial conditions specified as $\mathbf{x}(0)$. The state vector $\mathbf{x}$ is an $(n \times 1)$ vector and $\mathbf{u}$ is an $(m \times 1)$ control vector (reactants addition profiles) bounded by

$$u_{\min,i} \leq u_i \leq u_{\max,i}, \quad i = 1, 2, \ldots, m \tag{2}$$

The system may have n_i inequality constraints, and n_e equality constraints of the type

$$g_k(\mathbf{x}, \mathbf{u}) \leq 0, \quad k = 1, \ldots, n_i \tag{3}$$

$$h_k(\mathbf{x}, \mathbf{u}) = 0, \quad k = 1, \ldots, n_e \tag{4}$$

The multiobjective optimal control problem can now be stated, without loss of generality, to determine the optimal feed profiles $\mathbf{u}(t)$, in the time interval $0 \leq t \leq t_f$, which will simultaneously maximize a set of performance indices that depend on the final outcome of the process. This can be described mathematically as

$$\underset{\mathbf{u}(t)}{\text{Maximize}}\, \mathbf{J} \equiv \underset{\mathbf{u}(t)}{\text{Maximize}}\, [J_1(\mathbf{x}(t_f)), \ldots, J_s(\mathbf{x}(t_f))]^T \tag{5}$$

where $\mathbf{J}$ is a $(s \times 1)$ vector of the objective functions (performance indices) and t_f is the batch time of the crystallization.

Multiobjective Optimization by Genetic Algorithm

The solution and results of multiobjective function problems are conceptually different from single-objective function problems. In the case of multiple objectives, there may not exist one solution that is the best with respect to all objectives. The presence of multiple objectives in a problem usually gives rise to a family of nondominated or noninferior solutions, largely known as Pareto-optimal solutions, where each objective component of any solution along the Pareto front can only be improved by degrading at least one of its other objective components. Since none of the solutions in the nondominated set is absolutely better than any other, any one of these is an acceptable solution. As it is difficult to choose any particular solution for a multiobjective optimization problem without iterative interaction with the decision maker, one general approach is to establish the entire set of Pareto-optimal solutions. Extensive research has been reported in recent literature on the algorithms used for generating nondominated Pareto-optimal solutions. Among many multiobjective optimization approaches, methods based on evolutionary algorithms are the most popular because they

deal simultaneously with a set of possible solutions, and can generate the whole set of Pareto-optimal solutions in a single run of the algorithm rather than requiring an iterative process like traditional techniques. Additionally, evolutionary algorithms are less susceptible to the shape or continuity of the Pareto front. Some of the other advantages of evolutionary algorithms are that they require very little knowledge about the problem being solved, robust, and can be implemented in a parallel environment. The well known evolutionary multiobjective approach, the real-coded elitist nondominated sorting genetic algorithm or NSGA-II procedure,[18] has been adapted here for solution of constrained multiobjective optimal control problems that appear in a reactive crystallization process. The important features of NSGA-II are that it uses a fast nondominated sorting procedure, and an elite-preserving mechanism and, thereby, assuring preservation of previously found good solutions. Also, NSGA-II incorporates a simple yet efficient constraint-handling method, and it does not require any tunable parameter. Bhaskar et al.[19] have presented a detail review on several interesting multiobjective optimization problems in chemical engineering that have been solved by genetic algorithm and various other methods. Several interesting application of evolutionary multiobjective optimization in various chemical engineering problems can be found in recent literature.[16,20–26]

Implementation details of the algorithm

The first step in implementing any genetic algorithm (GA) is to decide how the decision variables should be encoded as strings, which are referred to as chromosomes (trial solutions). The feed addition policies must satisfy a terminal constraint: the total amount of feed added into the crystallizer must be exactly equal to the total amount of the fresh feed that is available. In order to handle this constraint, the amount of reactants added or volume (Q) against time is chosen here as control variable instead of the feed rate, F ($Q_i = \int_{t_0}^{t_f} C_{i,f} F_i dt$ or $Q_i = \int_{t_0}^{t_f} F_i dt$, where $C_{i,f}$ is the concentration of the component i in the feed).

To determine the optimal feed addition policy $Q_i(t)$, $i = 1, m$, we divide the time interval $[0, t_f]$ into P time stages of equal length (t_f/P), and seek a piecewise linear control policy for each reactant feed in the time interval (t_k, t_{k+1}) by

$$Q_i(t) = Q_i(k) + \frac{Q_i(k+1) - Q_i(k)}{t_f/P}(t - t_k) \qquad (6)$$

where $Q_i(k)$ is the value of Q_i at t_k. The optimal control problem then is to find the $Q_i(k)$, $k = 1, \ldots, P$. Since the initial amount of each reactant ($Q_i(0)$) is a decision variable, and the total amount of reactant i to be added is fixed at $Q_{i,\max}$, the number of variables that represent the piecewise linear feed addition profile for the entire feed addition duration is P. Thus, a chromosome can be represented by a real-valued vector of P values indicating the amount of feed on each equally spaced time partitions. These values are generated randomly in the initial population between the lower and upper bounds of the admissible values ($Q_i \in [Q_{i,\min}, Q_{i,\max}]$). The objective functions (*fitness functions*) can now be evaluated for each chromosome through the simulation of the model equations with the feed profile represented by the chromosome.

It may be noted that there are several constraints associated with the optimization problem. The final-time or endpoint inequality constraints (g_k) are easily handled by the penalty-parameterless approach in NSGA-II by using the binary selection operator, where two solutions are picked up from the population and the better solution is chosen as follows:

1. If both the solutions are feasible, choose the solution with better nondomination rank.
2. If one is feasible and other is not, choose the feasible solution.
3. If both the solutions are infeasible, choose the solution with smaller overall constraint violation.

Because of the transformation of the control variable (volume or amount of feed in place of feed rate), the equality constraints (h_k) in our case become equivalent to the upper bounds on the decision variables. The genetic operators (crossover, mutation) are so designed that solutions are always created within the specified lower and the upper bounds. Thus, the variable bounds will never be violated by NSGA-II during the course of optimization. However, the transformation of the control variable introduces an additional constraint on the feed addition profiles. Since we represent the amount of feed (volume) as decision variable, the feed addition profile must be a nondecreasing function of time. This constraint will be satisfied at all times if the decision variables representing a feed addition profile are always in ascending order. Generation of initial random population, as well as crossover and mutation operations during the evolution process, can both lead to nonordered set of decision variables. Therefore, an order maintaining procedure is included in the algorithm as an additional operator (*reorder operator*) to preserve the ascending nature of these variables.

We choose a fixed population size of 100 or 200 for all the problems considered in this study. The simulated binary crossover (SBX), and the polynomial mutation operators have been used with the probabilities of 0.9 and 0.05, respectively. The distribution index for the crossover operator is taken as 10, and that for mutation is chosen as 20 for all the cases. All the simulations are carried out for a predefined maximum number of generations (*iterations*), and the nondominated solutions of the final population are declared as the obtained Pareto-optimal solutions. All the computations are executed on a Sun Ultrasparc III computer. The details of the NSGA-II procedure can be found in Deb et al.,[18] and its adaptation for the present case studies is briefly outlined here as follows:

Step 1. Generate randomly a parent population $\mathcal{P}_0$ of size N using the chromosomal representation as discussed earlier.

Step 2. Check and restore the ascending order of the decision variables in the chromosomes.

Step 3. Evaluate each individual and classify them into several fronts ($\mathcal{F}_i$, $i = 1, 2, \ldots$.) by the fast nondominated sorting procedure.

Step 4. Generate child population $\mathcal{Q}_0$ from $\mathcal{P}_0$ by performing binary tournament selection, simulated binary crossover, and polynomial mutation.

Step 5. Check and restore the ascending order of the decision variables in the chromosomes.

Step 6. At any generation t, form a combined population $\mathcal{R}_t$ of size $2N$ by setting $\mathcal{R}_t = \mathcal{P}_t \cup \mathcal{Q}_t$, and perform nondominated sorting to identify different fronts $\mathcal{F}$ in $\mathcal{R}_t$.

Step 7. Create the new parent population $\mathcal{P}_{t+1}$ by adding the highest ranked front sets until the size of the population exceeds N using binary tournament selection, based on crowded comparison operator.

Step 8. Create the new child population $\mathcal{Q}_{t+1}$ from $\mathcal{P}_{t+1}$ by performing binary tournament selection, simulated-binary crossover, and polynomial mutation.

Step 9. Go to step 5 until the maximum number of allowable generation is reached.

Results and Discussions

Case study - I

We first consider a perfectly mixed, isothermal semibatch crystallizer as studied by Tavare and Garside,[12] and also by Choong and Smith,[15] where two feed streams, A and B, react together homogeneously to produce C, which then precipitates as solid crystal as the liquid phase becomes supersaturated with respect to component C. The chemical reaction is assumed to follow first-order kinetics with respect to each of the reacting components

$$A + B \longrightarrow C;\ \text{rate},\ r = k_r C_A C_B \tag{7}$$

and the mass-balance equations for the various components are described by the following differential equations

$$\frac{d(C_A V)}{dt} = C_{A,f} F_A - rV \tag{8}$$

$$\frac{d(C_B V)}{dt} = C_{B,f} F_B - rV \tag{9}$$

$$\frac{d(C_C V)}{dt} = rV - \frac{k_v \rho_c}{M_C} \frac{d(\mu_3 V)}{dt} \tag{10}$$

$$\frac{dV}{dt} = F_A + F_B \tag{11}$$

where C_i is the concentration of various reactive components, $C_{i,f}$ is the concentration of the component i in the feed stream, F_i is the feed rate, V is the capacity of the crystallizer, ρ_c is the density of crystals, k_v is the volume shape factor of the crystals, and μ_3 is the third moment of the CSD. Assuming that the crystallizer is well-mixed, crystal breakage and agglomeration are negligible, crystal growth is independent of size, and there is no growth rate dispersion, the properties of CSD can be described by the following moment differential equations[27]

$$\frac{d(\mu_0 V)}{dt} = B_N V \tag{12}$$

$$\frac{d(\mu_j V)}{dt} = j\mu_{j-1} G V, \quad j = 1, 2, 3, \ldots. \tag{13}$$

where μ_j represents the jth moment of the CSD. The nucleation rate kinetics, B_N and the growth-rate kinetics, G are described by the empirical power laws in supersaturation

$$B_N = k_b S^b = k_b (C_C - C_s)^b \tag{14}$$

$$G = k_g S^g = k_g (C_C - C_s)^g \tag{15}$$

where k_b, b, k_g, and g are the nucleation and growth rate parameters. S is the supersaturation defined in terms of a concentration difference as $S(t) = C_C - C_s$, where C_s is the equilibrium solute concentration.

Similar to nonreactive crystallization processes, the quality of a product CSD is usually described by its two main parameters: the WMS and the CV. The CV can be considered as a quantitative measure of the size spread of the product crystals. Thus, the desirable crystal characteristics are large WMS and low CV. We consider a multiobjective optimal control problem where we maximize the WMS (J_{11} = Maximize WMS), while simultaneously minimizing the CV (J_{12} = Minimize CV). The individual objectives ($\mathbf{J}_1 = [J_{11}, J_{12}]$) can be conveniently expressed in terms of the moments of the CSD,[27] and the multiobjective optimal control problem can be formally stated as follows

$$\begin{cases} \underset{Q_A(t), Q_B(t)}{\text{Maximize}} & J_{11} = \dfrac{\mu_4}{\mu_3} \\ \underset{Q_A(t), Q_B(t)}{\text{Minimize}} & J_{12} = \sqrt{\dfrac{\mu_3 \mu_5}{\mu_4^2} - 1} \\ \text{subject to} & g_1 = J_{11} \geq 16.1 \\ & g_2 = J_{12} \leq 18.0 \\ & g_3 = M_{\text{crystal}} \geq 3.87 \times 10^{-4} \\ & h_1 = Q_A(t_f) = 100 \\ & h_2 = Q_B(t_f) = 100 \end{cases} \tag{16}$$

The inequality constraints g_1, g_2, and g_3 allow the consideration of minimum desirable crystal size (16.1 μm), maximum allowable CV (18.0%), and a minimum desirable yield (3.87×10^{-4} kmol/kg), respectively. These values correspond to the properties of the product CSD obtained in an operation with constant rate of feeding. Thus, these constraints ensure that the results of the present study are better than those obtainable in operations with constant feed rate. The equality constraints (h_1, h_2) ensure that the total reactants added is exactly equal to the total amount of fresh feed that is available.

During the semi-batch operation, the reactants A and B are charged into the crystallizer in a period of 6,000 s, and then the crystallizer operates in a batch mode until 10,000 s.[12] The parameters for physical properties, reaction and crystallization kinetics of the system are given in Table 1. Following Choong and Smith,[15] we consider two different cases: double feeds with the same addition rates, and double feeds with different addition rates.

Double feeds with same addition profiles. Let us first consider the case where both the reactant streams follow exactly the same trajectory. To seek a piecewise linear control policy for A or B, we divide the feed addition period (6,000 s) into 12 equal intervals, and each chromosome is then represented by a real-valued vector of 12 values, indicating the amount (volume) of the feed on each equally spaced time partitions. The application of the multiobjective optimization algorithm with the NSGA-II parameters as discussed in the previous section, a population size of 100, and for a maximum generations of 2,000 (taking a CPU time of

Table 1. Parameters for Physical Properties, Reaction and Crystallization Kinetics of the System[15]

k_r, kg/kmol s	100
C_s, kmol/kg	1×10^{-4}
k_b, no./[kg s(mol/kg)^b]	3.1×10^{10}
b	4.5
k_g, m/[s(mol/kg)^g]	7.5×10^{-8}
g	1.5
k_v	0.52
ρ_c, kg/m^3	2000
M_C	100
$C_{A0} = C_{B0}$, kmol/kg	1×10^{-3}
Amount of reactant A, kg	100
Amount of reactant B, kg	100

1,363 s) resulted in the Pareto-optimal front presented in Figure 1. A well-defined Pareto-optimal front was obtained within 50 generations (taking a CPU time of 35 s) as can be seen from Figure 2 which shows the evolution of the Pareto-optimal front at different generations as the algorithm progresses. The algorithm can identify the Pareto-optimal front very quickly, and also has the capability of maintaining a sustainable wide-spread population over the entire Pareto-optimal region in subsequent generations. The Pareto-optimal front is a combination of equally competitive solutions, and the trade-off obtained between the two objectives is clear from Figure 1. The WMS of the crystals can be improved only at the expense of increased CV, which is undesirable. Although the CV increases monotonically with increase in WMS, the rate of increase in CV becomes faster at higher values of WMS. The decision maker can choose one solution out of this set of solutions by either using his/her intuition or using some higher level information. The Pareto-optimal front shown in Figure 1 consists of two distinct regions. The lower end of the Pareto-optimal front (region I) is characterized by relatively slow increase in the CV, with increase in the WMS of crystals up to about WMS = 21 μm. On the other hand, the upper end of the Pareto-optimal front (region II) is characterized by a more rapid and almost linear increase in CV, with increase in WMS. The sensitivity and the geometry of the optimal region can, thus, be easily assessed from the Pareto-optimal front. For example, Figure 1 reveals that crystals with a WMS of 18.9 μm can be produced with a corresponding CV of 11.6%. But a small tolerance in CV from 11.6% to 12.8% would yield a CSD with WMS of 21.4 μ. The evolution of the entire Pareto-optimal solutions in a single run of the algorithm immediately points out to the decision maker the whole range of WMS that can be achieved, and the undesirable CV that would be associated with it. The solution of the single-objective optimization problem does not yield such useful information about the relationship among the several objective criteria, and a set of decision variables so readily. Thus, the multiobjective optimization approach enables the decision maker to identify the best feasible solution in full knowledge of other alternative solutions.

In order to verify whether the obtained solutions are close to the true Pareto-optimal front of this problem, we combine the different objective functions into a single performance criterion through a weighted linear combination of different objectives, and solve it repeatedly with different settings of the weights by a single-objective GA. The GA parameters, such as the population size, operator parameters, and so on, are kept the same as those used in the multiobjective optimization study. The solutions to the problem are shown in Figure 1 marked as circles. Since these solutions are found to

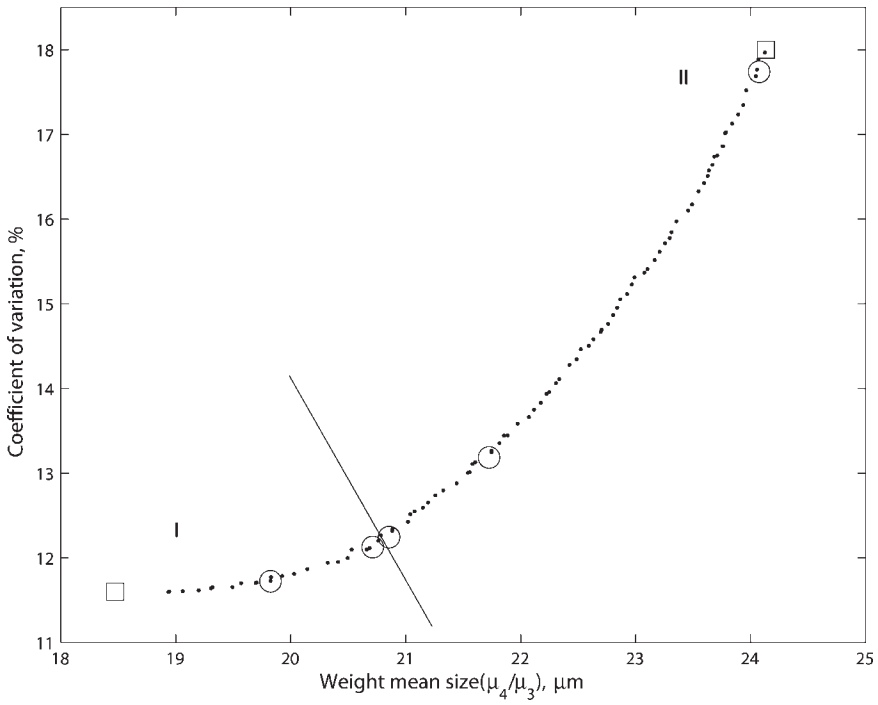

Figure 1. Pareto-optimal front for case study I: double feeds with same addition profiles.

The squares represent the results of single-objective optimization of individual objective functions. The circles represent the results of several single-objective optimization using weighted linear combination of all the objectives.

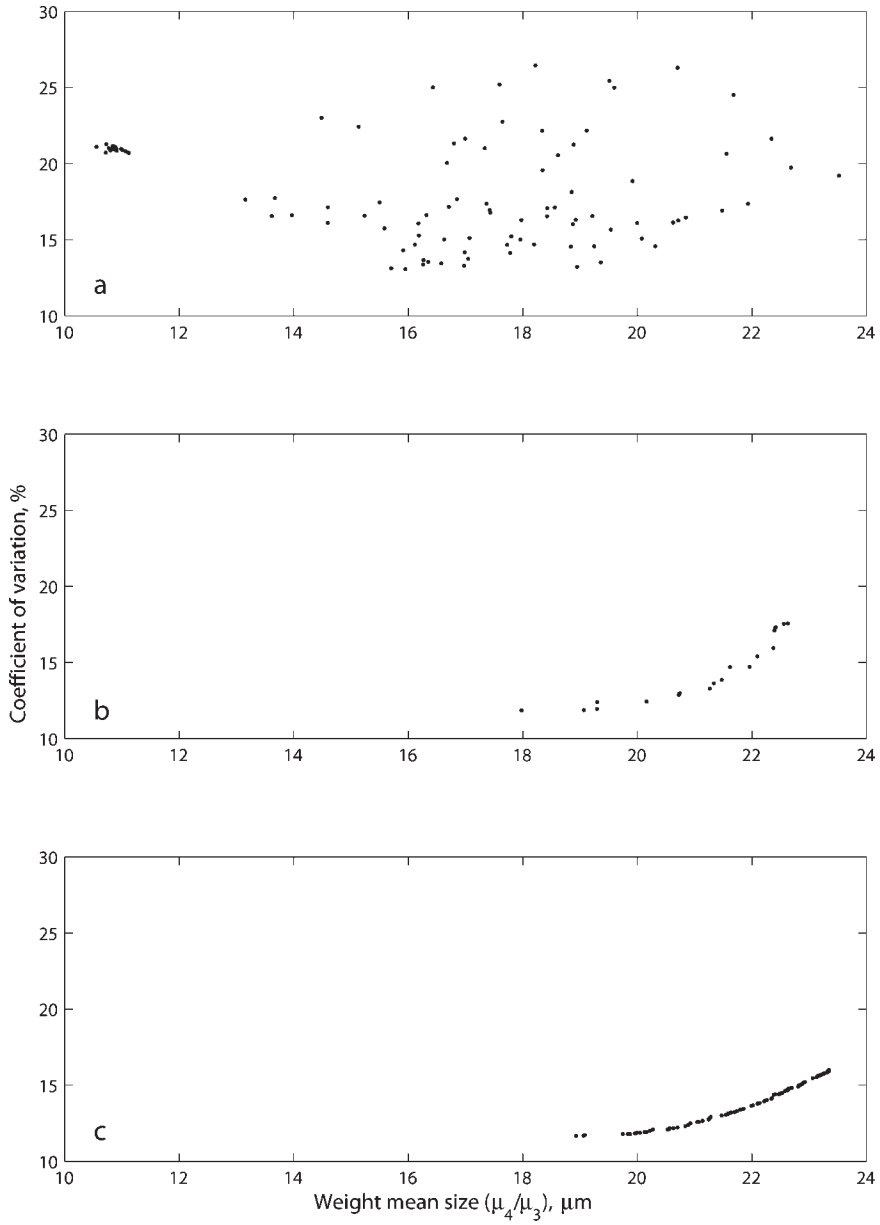

Figure 2. The evolution of the Pareto-optimal front in Figure 1.

(a) Random initial population, (b) distribution of feasible solutions at generation number 10, and (c) distribution of feasible solutions at generation number 50.

lie on the Pareto-optimal front obtained in the multiobjective approach, it can be stated that the solutions obtained using multiobjective approach constitute the true Pareto-optimal front for the problem. The results of the single-objective optimization of the individual objective functions (subject to the constraints g_k and h_k) using a single-objective GA are also shown on Figure 1 marked as squares located at the lower end and the upper end of the Pareto-optimal front. Thus the single-objective formulations of the multiple objective problem yield the "extreme" solutions.

Each point of the Pareto-optimal front in Figure 1 is associated with a different feed addition profile having different initial amounts of reactants. However, the general features of the policies are slow addition at the beginning, and fast addition toward the end of the addition time. Some representative feed addition profiles taken from different ends of the Pareto-optimal front in Figure 1, are shown in Figure 3a. A feed profile taken from the lower end of the Pareto-optimal front (region I) should correspond to the solution of the problem where we want to minimize the CV alone. The feed profile yields a WMS of 18.9 μm with a CV of 11.6%. Similarly, a typical feed profile corresponding to the higher end of the Pareto front (region II), should correspond to the case where we want to maximize the WMS alone. The feed profile yields a WMS of 24.1 μm with a CV of 17.9%. These values are in good agreement with the results of single objective optimization study by Choong and Smith.[15] The feed profiles corresponding to all the other Pareto-optimal solutions

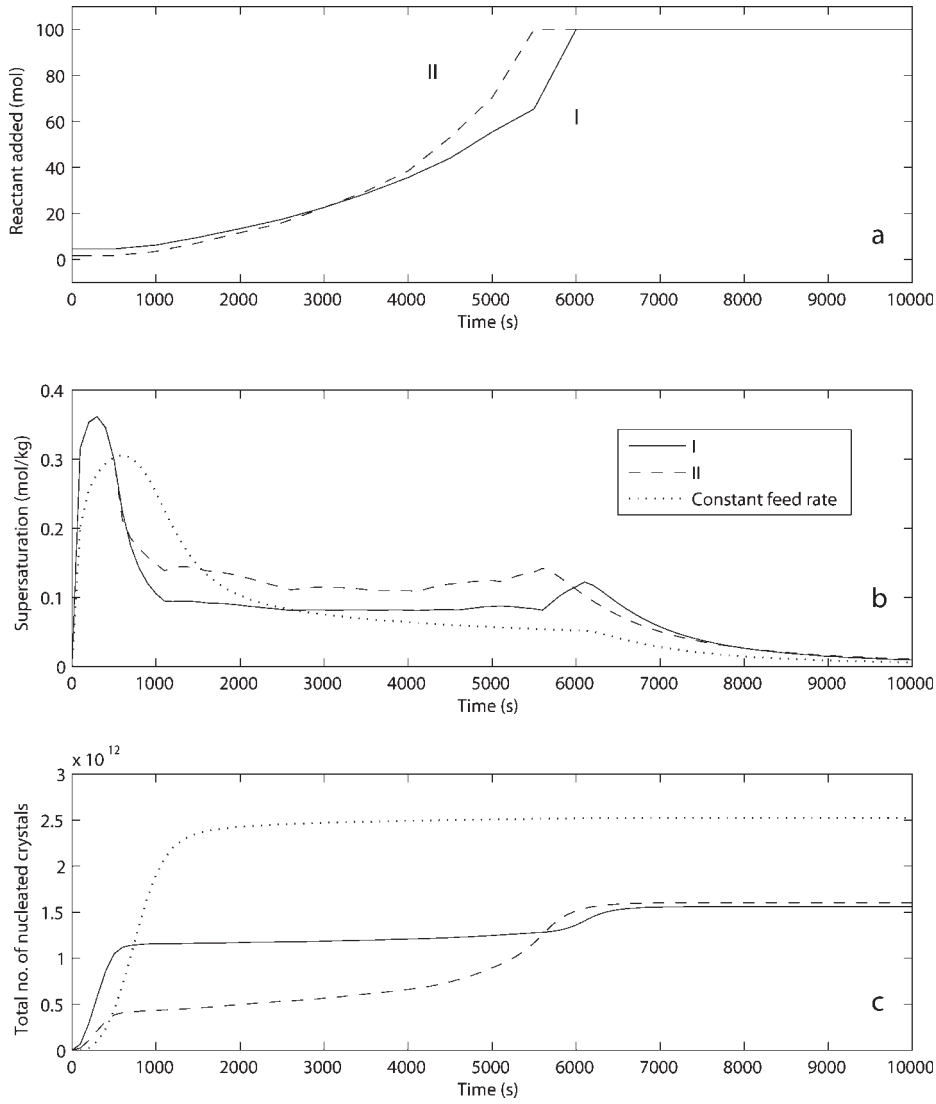

Figure 3. Feed profiles (a), the associated supersaturation profiles (b), and variation of total number of crystals (c) corresponding to different Pareto-optimal solutions taken from different regions (as indicated by I and II) of the Pareto-optimal front in Figure 1 and a constant feeding rate.

remain within the space encompassed by these two profiles represented by I and II. The effect of optimal initial amounts of reactants on WMS and CV of the product CSD, are presented in Figure 4. Increased amount of initial reactants cause a decrease in both WMS and CV, but the WMS decreases almost linearly with increase in the initial amounts of the reactants.

Figure 3b shows the trajectories of the supersaturation in the crystallizer corresponding to the feed profiles presented in Figure 3a, and for a constant rate of feed addition. It may be noted that both the feed trajectories I and II lead to an early increase in supersaturation to almost the same extent to produce an adequate number of crystals. However, they produce different numbers of crystals in the beginning (Figure 3c) due to different initial amounts of reactants associated with the profiles. During the subsequent growth phase, the supersaturation is maintained at different levels to produce CSD with different characteristics. Minimizing CV requires the supersaturation level to be maintained at lower level than maximizing the WMS.

Figure 3c shows the variation of the number of the crystals with time for the three different feed profiles. The constant rate of feed addition produces the largest number of nucleated crystal and almost all the crystals are nucleated at the beginning of the operation. Minimizing the total number of crystals should increase the final average size of the crystals for a given crystal yield. Both the feed profiles I and II produce almost the same number of total nucleated crystals and yield. However, they follow a different trajectory for production of nucleated crystals. The profile that preferentially minimizes the CV has almost all the crystals nucleated at the beginning of the operation, whereas the profile that preferentially maximizes the WMS has the crystals being nucleated continuously during the entire feed addition period.

The optimization studies carried out in this study are subjected to the constraints of minimum desirable WMS, mini-

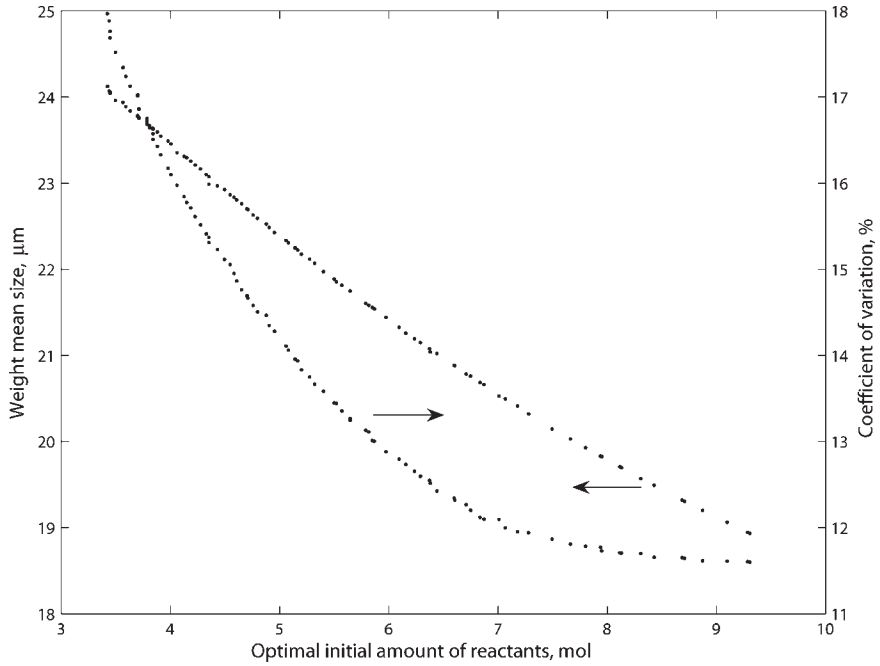

Figure 4. Effect of optimal initial amount of reactants on the WMS and the CV of the crystals.

mum desirable yield, and maximum allowable CV. Figure 5 presents the much extended Pareto-optimal fronts that are obtained when we remove some (remove g_1, g_2, and keep only the minimum yield constraint g_3) or all of these constraints (remove g_1, g_2, g_3). The importance of the constraint on the yield is obvious from the figure. The figure also presents two additional Pareto-optimal fronts that are obtained when simulations are carried out for the original constrained problem with the values of the kinetic parameters b changed from 4.5 to 4.0, and the value of g changed from 1.5 to 1.2. The sensitivity of the Pareto-optimal front on the values of the kinetic parameters b and g is clear from the figure. The spread of WMS and CV changes widely due to differences in nucleation and growth rates, but the general qualitative features of the Pareto optimal fronts remain the same.

Double feeds with different addition profiles. Let us now consider the case where the feed profiles corresponding to different reactant streams may have different trajectories. We again divide the feed addition period (6,000 s) into 12 equal intervals, and each chromosome can, thus, be represented by a vector of 24 real numbers where the first 12 numbers represent the feed policy for the reactant *A*, and the next 12 represent that for the reactant *B*. The application of the multiobjective optimization algorithm with a population size of 200, and for a maximum generations of 2,000 (taking a CPU time of 4,045 s) produces the results that are presented in Figure 6 and Figure 7.

The general features of the Pareto-optimal front are similar to those obtained for double feeds with same addition policies. However, the feed profiles evolved for reactants *A* and *B* are different. Although the policies for reactant *B* show the same slow addition at the beginning and fast addition towards the end, the feed policies for reactant *A* show a distinct behavior as we move along the Pareto-optimal front. The optimal policies for *A* from the lower end of the Pareto-optimal front start with a fast addition at the beginning, then they follow a batch period, and finally end with a fast addition. The time at which the batch period starts, and its duration decrease as we go from the lower end of the Pareto-optimal front (preferential minimization of CV) to the upper end of the front (preferential maximization of WMS). For example, the optimal feed profile for *A* from the extreme lower end of the Pareto-optimal front starts with 7 mol of initial reactants and charges about 21 mol of *A* within 1,000 s. Then it goes through a batch period until about 3,200 s, after which it is again fed continuously until the end. Another feed profile from the front (with WMS = 20.5 μm, CV = 11.7%) starts with an initial amount of 5 mol, charges about 12 mol of *A* within 700 s, and then goes to a batch mode till 2,100 s, after which a continuous feeding starts until the end. On the other hand, the optimal feed profile from the upper end of the Pareto-optimal front has an initial amount of 2 mol of *A*, and starts with a batch period until of 700 s, after which it is fed continuously until all the reactants are fed at 5,500 s. Choong and Smith[15] reported that while optimizing the CV subject to a minimum WMS, the entire amount of the reactant *A* (100 mol) was charged within 352 s of the operation and the other reactant was charged continuously. Thus, one reactant was fed as a single charge in their study.

Case study - II

The precipitation of barium sulfate from aqueous feed streams of barium chloride and sodium sulfate has been extensively studied for studies on nucleation, growth kinetics, and mixing effect on product CSD. This case study is again based on that in Choong and Smith[15] so that the results of multiobjective approach in this work could be compared against their single-objective optimization results using a simulated-annealing based method. A semibatch operation is

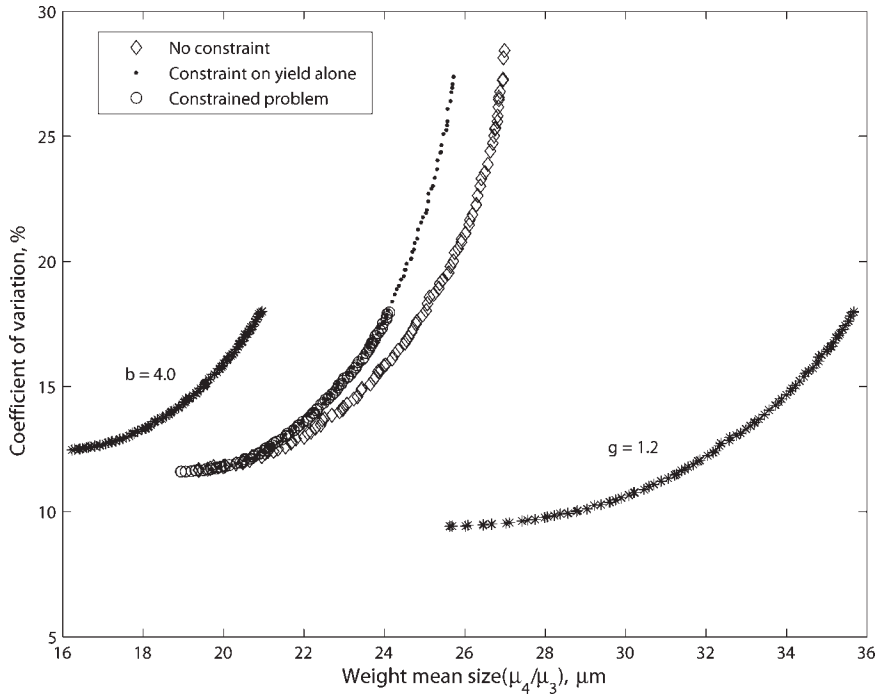

Figure 5. Pareto-optimal fronts for maximization of the WMS and minimization of the CV with some (g_1, g_2), or all the constraints (g_1, g_2, g_3) removed.

Pareto-optimal fronts obtained with changed kinetic parameters (b,g) are also shown.

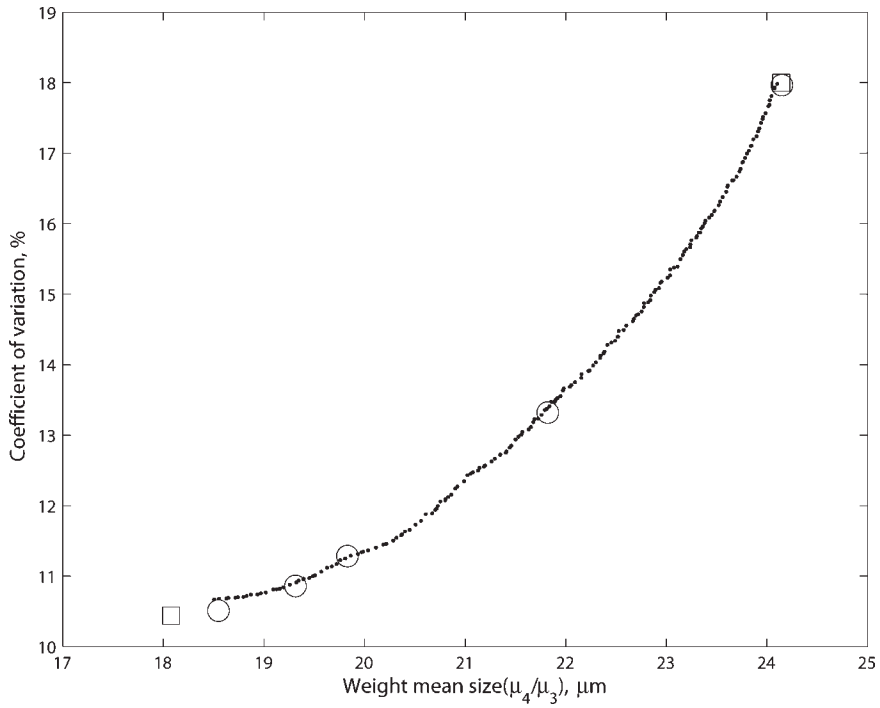

Figure 6. Pareto-optimal front for case study I: double feeds with different addition profiles.

The squares represent the results of single-objective optimization of individual objective functions. The circles represent the results of several single-objective optimization using weighted linear combination of all the objectives.

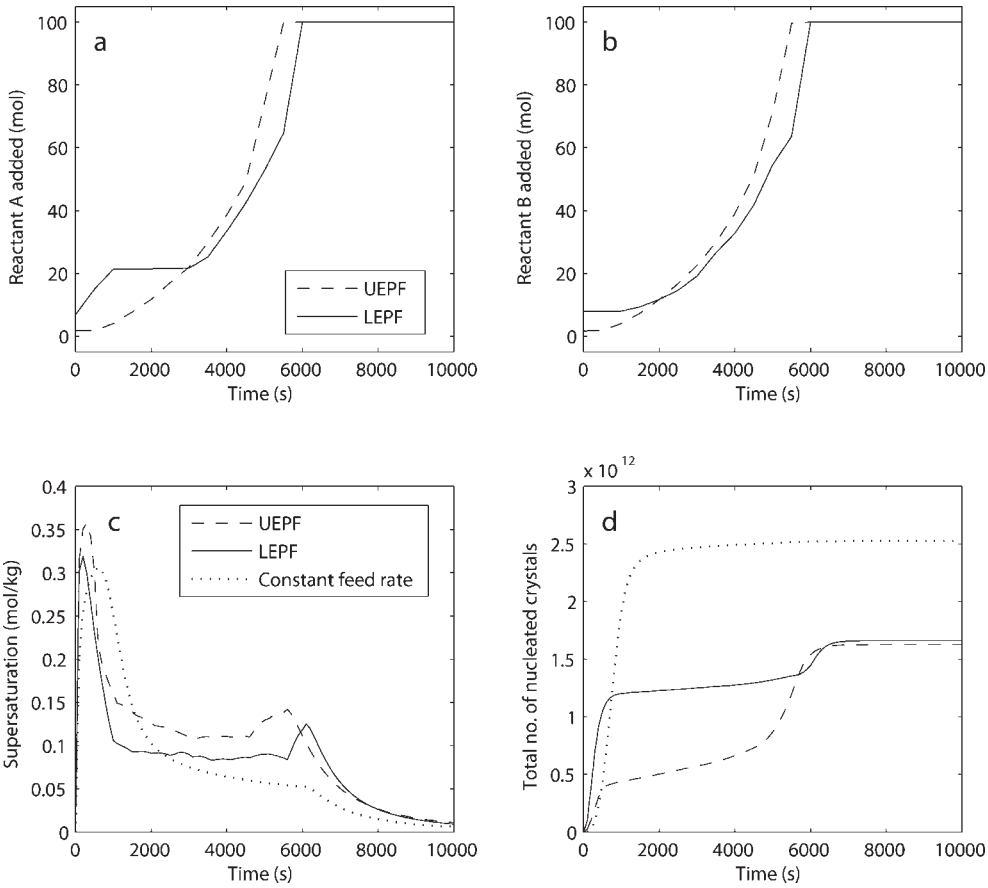

Figure 7. (a) Feed profiles for reactant *A*, (b) feed profiles for reactant *B*, (c) the supersaturation profiles associated with different profiles, and (d) variation of total number of crystals corresponding to different feed profiles.

LEPF: Lower end of the Pareto-optimal front, UEPF: Upper end of the Pareto-optimal front.

highly desirable for the fast ionic precipitation of sparingly soluble barium sulfate, as the chemical reaction involved is instantaneous and nucleation is rapid. The chemical reaction can be described as

$$BaCl_2 + Na_2SO_4 \rightarrow BaSO_4\downarrow \tag{17}$$

and the mass-balance equations for the various components can be described as follows

$$\frac{d(C_{Ba^{2+}}V)}{dt} = C_{Ba^{2+}f}F_{Ba^{2+}} - \frac{k_v\rho_c}{M_{BaSO_4}}\frac{d(\mu_3 V)}{dt} \tag{18}$$

$$\frac{d(C_{SO_4^{2-}}V)}{dt} = C_{SO_4^{2-}f}F_{SO_4^{2-}} - \frac{k_v\rho_c}{M_{BaSO_4}}\frac{d(\mu_3 V)}{dt} \tag{19}$$

$$\frac{d(C_{BaSO_4}V)}{dt} = \frac{k_v\rho_c}{M_{BaSO_4}}\frac{d(\mu_3 V)}{dt} \tag{20}$$

$$\frac{dV}{dt} = F_{Ba^{2+}} + F_{SO_4^{2-}} \tag{21}$$

The properties of the CSD are described by the moment differential equations as before by Eqs. 12 and 13. The nucleation-rate kinetics B_N, and the growth-rate kinetics G, are now described as

$$B_N = B^0 \exp(-A_N/\ln^2 S_a) \tag{22}$$

$$G = k_g(1 - S_a)^g \tag{23}$$

where S_a is the thermodynamic supersaturation ratio defined as[8,17,28]

$$S_a = (c_+^{v+}c_-^{v-}/K_{sp})^{1/v} \tag{24}$$

where c_+ and c_- refer to the concentrations of the cation and anion that are formed from the product crystal when it dissociates in the solution. v^+ and v^- are the number of moles of cations and anions in 1 mol of solute, and v refers to the number of mole of ions in 1 mol of solute. The crystallization kinetics and physical properties of the barium sulfate system are given in Table 2.

A total of 2.46×10^{-3} m^3 of reactive solution of sodium sulfate is initially present in the tank. A total of 40×10^{-6} m^3 of a barium chloride solution is to be fed into the vessel over a given batch time of 180 s. The feed concentration of

Table 2. Precipitation Kinetics and Physical Properties for Barium Sulfate System[15]

For $S_a \geq 10^3$	
A_N	2686
B_0, no./(m^3 s)	10^{36}
For $S_a < 10^3$	
A_N	67.3
B^0, no./(m^3 s)	1.46×10^{12}
k_g, m/s	4.0×10^{-11}
g	2
K_{sp}, kmol^2/m^6	1.10×10^{-11}
ρ_c, kg/m^3	4480
k_v	$\pi/6$
M_{BaSO_4}	233.4

barium chloride is fixed at 1.0 kmol/m^3, and the initial concentration of sodium sulfate is fixed at 0.01626 kmol/m^3. Similar to case study I, we again consider a multiobjective optimal control problem where we maximize the WMS, while simultaneously minimizing the CV ($\mathbf{J}_2 = [J_{21}, J_{22}]$). The same definitions of the WMS and the CV as used in Wei et al.,[8] Choong and Smith[15] are used here for the purpose of comparison

$$\begin{cases} \underset{Q_{BaCl_2}(t)}{\text{Maximize}} & J_{21} = \dfrac{\mu_3}{\mu_2} \\ \underset{Q_{BaCl_2}(t)}{\text{Minimize}} & J_{22} = \sqrt{\dfrac{\mu_2\mu_0}{\mu_1^2} - 1} \\ \text{subject to} & g_1 = J_{21} \geq 11.1 \\ & g_2 = J_{22} \leq 56.6 \\ & h_1 = Q_{BaCl_2}(t_f) = 40 \times 10^{-6} \end{cases} \tag{25}$$

Again the minimum desirable crystal size (11.1 μm), and the maximum allowable CV (56.6%) correspond to the properties of the product CSD obtained in an operation with constant rate of feeding.

To seek a piecewise linear control policy for barium chloride addition, we divide the given batch time (180 s) into 10 equal intervals, and each chromosome is then represented by a vector of 10 real numbers. The application of the multiob-

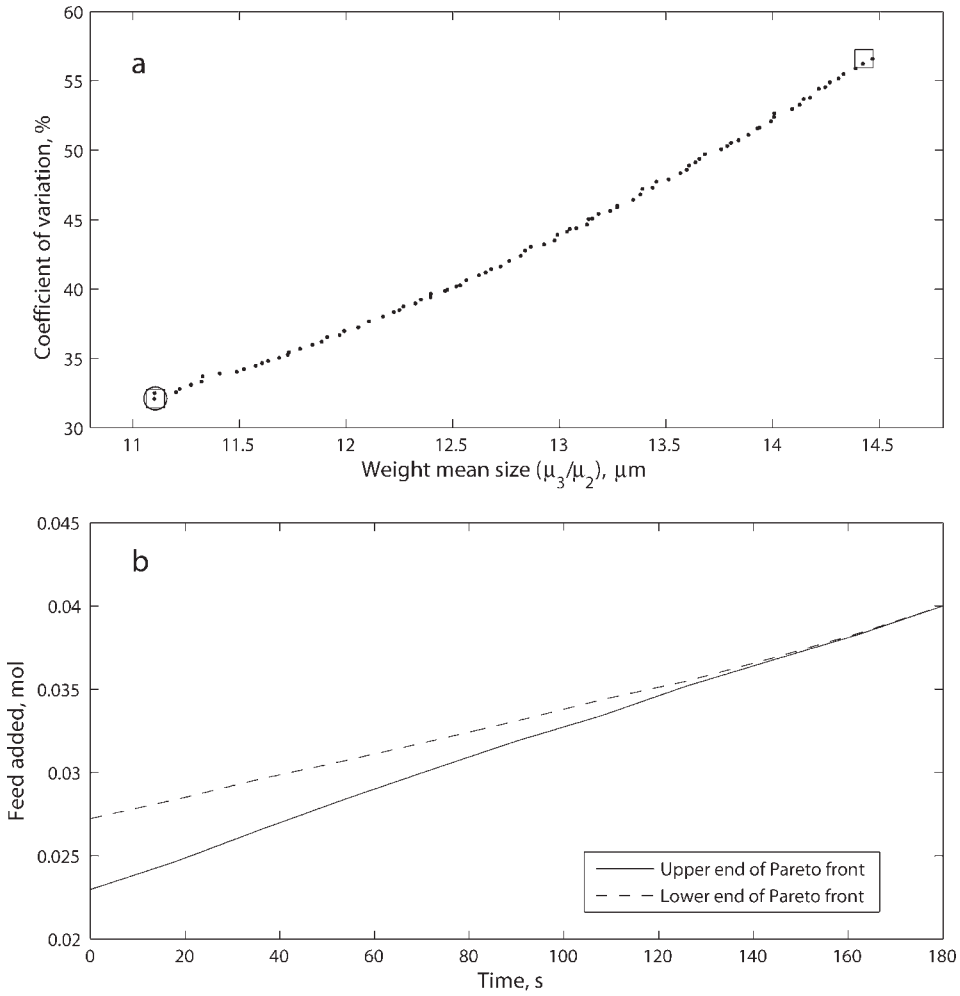

Figure 8. (a) Pareto-optimal front for case study II and (b) feed profiles for barium chloride corresponding to solutions taken from lower and upper ends of the Pareto front.

The squares represent the results of single-objective optimization of individual objective functions. The circles represent the results of several single-objective optimization using weighted linear combination of all the objectives.

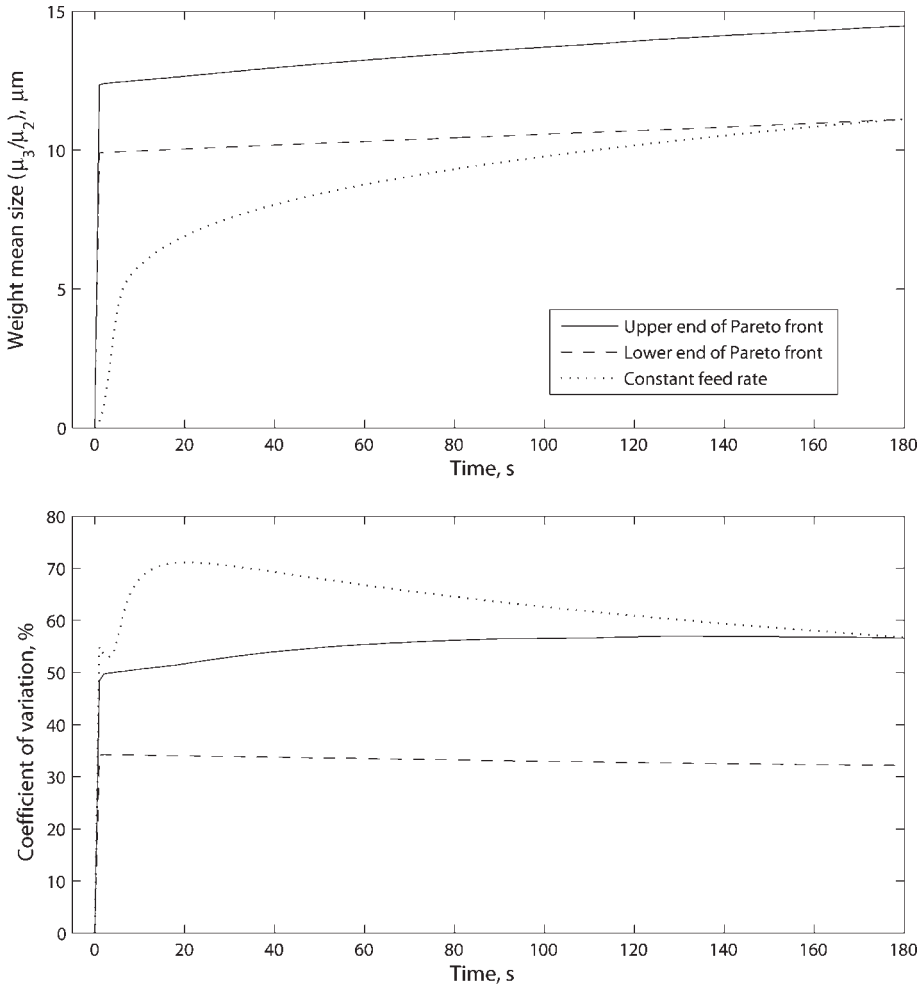

Figure 9. Variation of the WMS and the CV of the crystals with time for different feed profiles for barium sulfate precipitation.

jective optimization algorithm with a population size of 100, and for a maximum generations of 1,000 (taking a CPU time of 1,997 s) produces the results that are presented in Figure 8 and Figure 9. The Pareto-optimal front obtained for this case study (Fig. 8a) is almost linear and the CV increases monotonically with increase in WMS with almost a constant rate. The solutions to the single-objective optimization of the individual objective functions subject to the given constraints are shown on Figure 8a marked as squares located at both ends of the Pareto-optimal front. The solutions to the problem with weighted linear combination of different objectives are also shown on Figure 8a marked as circles. All the linear combinations here yield only one solution on the Pareto-optimal front that corresponds to the preferential minimization of the CV alone. Some representative feed profiles taken from different ends of the Pareto-optimal front are shown in Figure 8b. The feed profiles corresponding to all the other Pareto-optimal solutions remain within the space encompassed by these two profiles. All the profiles vary almost linearly with time. However, each feed policy is associated with a different initial amount of barium chloride, and, therefore, the initial amount of the reactant plays a very important role in the final achievable CSD. A feed profile taken from the lower end of the Pareto-optimal front (preferential minimization of CV), has an initial barium chloride of 0.027 mol, and yields a CSD with WMS of 11.1 μm with a CV of 32.1%. On the other hand, a feed profile corresponding to the higher end of the Pareto front (preferential maximization of WMS), has an initial barium chloride of 0.023 mol, and yields a CSD with WMS of 14.5 μm with a CV of 56.6%. These values are in good agreement with the results of single objective optimization study by Choong and Smith.[15]

Figure 9 presents the variation of the WMS and the CV of the crystals as time progresses for different feed profiles. The optimal feed profiles increase the WMS of the crystals very rapidly at the early stage of the operation, due to the instantaneous nature of the reaction. About 85–89% of the final achievable WMS is obtained within 1 s of the operation for the two optimal solutions shown. A similar trend in an early increase in the CV is also observed for all the profiles. The effect of optimal initial amount of barium chloride on WMS and CV of the product CSD are presented in Figure 10.

Table 3 lists the characteristic features of some of the solutions (operating conditions) that are evolved as optimal in the present study with that of a constant feed rate profile. It may be noted that all the profiles evolved in this study are bet-

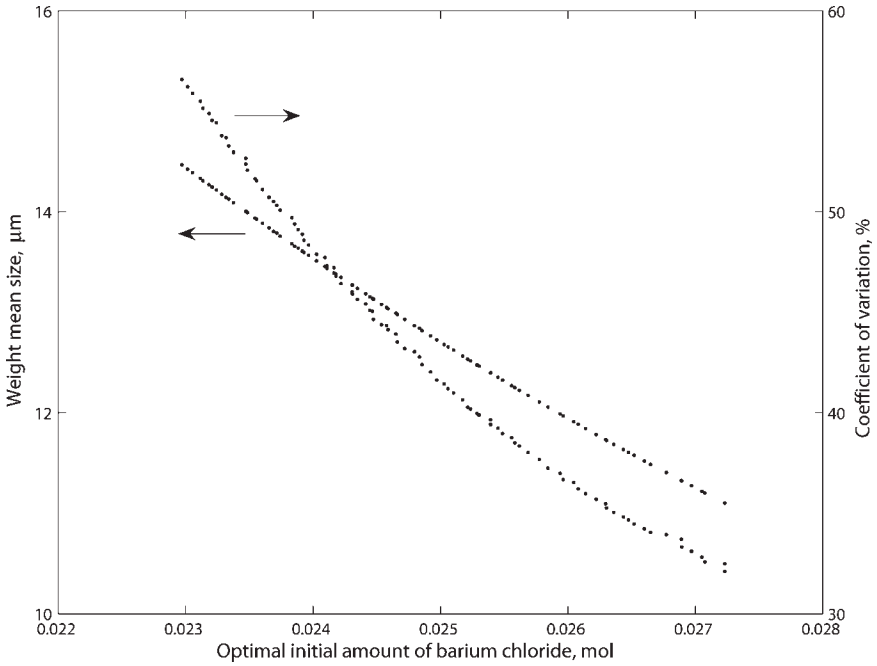

Figure 10. Effect of optimal initial amount of barium chloride on the WMS and the CV of the crystals for barium sulfate precipitation.

ter than the constant feed profile, when both the objective functions are considered simultaneously. To further compare the performances of the obtained Pareto-optimal solutions with the constant feed rate profile, simulations are carried out with the constant feed rate profile and the different amounts of initial reactants that are evolved as optimal solutions in our multiobjective approach. The performances in terms of the achievable WMS and CV (data not shown) of the constant-feed rate profiles are almost same as that of the evolved optimal solutions for case study II. This is expected as the optimal solutions also have almost constant rate of addition with different amounts of initial reactants. However, the performances of constant feed profiles are much inferior compared to their optimally found counterparts for case study I.

Conclusions

Semibatch operation for a reactive crystallization process offers the advantages of easily controllable feed-flow rates of reactants, which can lead to significant improvement in product quality than traditional batch operation. Thus, the determination of the optimal feed profiles for a reactive crystallizer is an important dynamic optimization problem. Crystallization processes typically have multiple performance objectives some of which compete with each other. The presence of multiple objectives in a problem usually gives rise to a set of optimal solutions, commonly known as *Pareto-optimal* solutions. Therefore, the optimization problems require simultaneous consideration of multiple objectives for best process operation. This study demonstrates the potential for multiobjective optimization approach for a semibatch reactive crystallization process. The well known evolutionary multiobjective approach, the real-coded elitist nondominated sorting genetic algorithm or NSGA-II procedure has been adapted to obtain the Pareto-optimal solutions for constrained multiobjective optimization problems that are related to the quality of product CSD in reactive crystallizers. The evolution of the entire Pareto-optimal front can help the designer visualize the trade-offs between different objectives, and select an appropriate operating condition for the process.

By employing the multi-objective optimization approach in a semibatch reactive crystallization process, insights and guidelines are obtained regarding the optimal operation of the crystallizer to obtain crystals of desired characteristics. In particular, the treatment analyzes how the feed flow rates of the reactants need to be tuned to reach an optimal compromise between the mean crystal size and the size distribution width. The knowledge of all the trade-off solutions is highly

Table 3. Comparison between Simulation Results under Different Operating Conditions

Feed profile	WMS (μm)	CV (%)
Figure 1	18.9	11.6
	19.5	11.6
	24.1	17.9
	20.3	11.8
	21.4	12.8
	21.0	12.4
Figure 6	24.1	17.9
	18.5	10.6
	23.5	16.2
	19.0	10.7
	22.6	14.5
	21.2	12.6
Figure 8a	14.5	56.6
	11.1	32.1
	12.2	38.0
	13.5	47.8
Constant feed (Case study I)	16.0	18.0
Constant feed (Case study II)	11.1	56.6

informative in real-world design activities, and may also provide guidelines for experimental investigation. Additionally, the optimal control strategies obtained in this study can be used as the starting point in a more rigorous simulation which accounts for the effect of various mixing and fluid dynamics by integrating computational-fluid dynamics with the population-balance equations, and the mixing models.

Notation

b = exponent relating nucleation rate to supersaturation
B_N = crystal nucleation rate, number/(kg solvent s)
C_s = solubility of the solute, kg solute/kg solvent
CSD = crystal-size distribution
CV = coefficient of variation
g = exponent relating growth rate to supersaturation
g_i = ith inequality constraints of an optimization problem
G = crystal-growth rate, m/s
h_i = ith equality constraints of an optimization problem
$\mathbf{J}_i$ = objective function vector of the ith case study
J_{ij} = jth objective function for the ith case study
k_b = nucleation-rate constant
k_g = growth-rate constant
k_r = reaction-rate constant
K_{sp} = solubility product
k_v = volumetric shape factor
M_{crystal} = mass of the crystal produced, kmol/kg solvent
S = supersaturation
t_f = final time, s
WMS = weight mean size

Greek letters

μ_i = ith moment of the CSD, number μ^i/kg solvent
ν = number of moles of ions in 1 mol of solute
ν^+ = number of moles of cation in 1 mol of solute
ν^- = number of moles of anion in 1 mol of solute
ρ_c = density of crystals, kg/m^3

Subscripts/superscripts

max = maximum
min = minimum

Acknowledgment

The financial support from the Natural Sciences and Engineering Research Council (NSERC) of Canada is gratefully acknowledged.

Literature Cited

1. Nielsen AE. *Kinetics of precipitation*. Oxford: Pergamon; 1964.
2. Nyvlt J, Sohnel O, Matuchova M, Broul M. *The kinetics of industrial crystallization*. Amsterdam: Elsevier; 1985.
3. Mersmann A, Kind M. Chemical engineering aspects of precipitation from solution. *Chem Eng Technol*. 1988;11:264–276.
4. Sohnel O, Garside J. *Precipitation: basic principles and industrial application*. Oxford: Butterworth-Heinemann Ltd.; 1992.
5. Franke J, Mersmann A. The Influence of operating conditions on the precipitation process. *Chem Eng Sci*. 1995;50:1737–1753.
6. Tavare NS. *Industrial crystallization: process simulation, analysis and design*. New York: Plenum; 1995.
7. Berry DA, Ng KM. Synthesis of reactive crystallization processes. *AIChE J*. 1997;43:1737–1750.
8. Wei H, Zhou W, Garside J. Computational fluid dynamics modeling of the precipitation process in a semi-batch crystallizer. *Ind and Eng Chem Res*. 2001;40:5255–5261.
9. Tadayyon A, Arifuzzaman SM, Rohani S. Reactive Crystallization of brushite under steady state and transient conditions: modeling and experiment. *Ind and Eng Chem Res*. 2003;42:6774–6785.
10. Torbacke M, Rasmuson AC. Mesomixing in semi-batch reaction crystallization and influence of reactor size. *AIChE J* 2004;50:3107–3119.
11. Torbacke M, Rasmuson AC. Influence of different scales of mixing in reaction crystallization. *Chem Eng Sci*. 2001;56:2459–2473.
12. Tavare NS, Garside J. Simulation of reactive precipitation in a semi-batch crystallizer. *Trans of Inst of Chem Eng*. 1990;68:115–122.
13. Mukhopadhyay SC, Epstein MAF. Computer model for crystal size distribution control in a semi-batch evaporative crystallizer. *Ind and Eng Chem Proc Design Development*. 1980;19:352–358.
14. Philips R, Rohani S, Baldyga J. Micro-mixing in a single-feed semi-batch precipitation process. *AIChE J*. 1999;45:82–92.
15. Choong KL, Smith R. Optimization of semi-batch reactive crystallization processes. *Chem Eng Sci*. 2004;59:1529–1540.
16. Sarkar D, Rohani S, Jutan A. Multi-objective optimization of seeded batch crystallization processes. *Chem Eng Sci*. 2006;61:5282–5295.
17. Zauner R, Jones AG. Mixing effects on product particle characteristics from semi-batch crystal precipitation. *Chem Eng Res and Design*. 2000;78:894–901.
18. Deb K, Pratap A, Agarwal S, Meyarivan T. A fast and elitist multi-objective genetic algorithm: NSGA-II. *IEEE Trans on Evolutionary Comp*. 2002;6:182–197.
19. Bhaskar V, Gupta SK, Ray AK. Applications of multi-objective optimization in chemical engineering. *Rev in Chem Eng*. 2000;16:1–54.
20. Kasat RB, Gupta SK, Kunzru D, Saraf DN. Multi-objective optimization of industrial FCC units using elitist nondominated sorting genetic algorithm. *Ind and Eng Chem Res*. 2002;41:4765–4776.
21. Zhang Z, Hidajat K, Ray AK, Morbidelli M. Multi-objective optimization of SMB and Varicol process for chiral separation. *AIChE J*. 2002;48:2800–2816.
22. Immanuel CD, Doyle III FJ. Hierarchical multi-objective strategy for particle-size distribution control. *AIChE J*. 2003;49:2383–2399.
23. Silva CM, Biscaia Jr. EC. Genetic algorithm development for multi-objective optimization of batch free-radical polymerization reactors. *Comp and Chem Eng*. 2003;27:1329–1344.
24. Deb K. Mitra K, Dewri R, Majumdar S. Towards a better understanding of the epoxy-polymerization process using multi-objective evolutionary computation. *Chem Eng Sci*. 2004;59:4261–4277.
25. Sarkar D, Modak JM. Pareto-optimal solutions for multi-objective optimization of fed-batch bioreactors using nondominated sorting genetic algorithm. *Chem Eng Sci*. 2005;60:481–492.
26. Yu W, Hidajat K, Ray AK. Optimization of reactive simulated moving bed and Varicol systems for hydrolysis of methyl acetate. *Chem Eng J*. 2005;112:57–72.
27. Randolph AD, Larson MA. *Theory of particulate processes*. 2nd ed. New York: Academic Press; 1988.
28. Mullin JW. *Crystallization*. 4th Ed. Oxford: Butterworth-Heinemann, 2001.

Manuscript received Jun. 21, 2006, and revision received Jan. 23, 2007.